

Geophysical Research Letters®

RESEARCH LETTER

10.1029/2021GL096377

Key Points:

- Extreme persistent rainfall in boreal summer 2020 over Northeast Indian subcontinent was the second heaviest on record since 1901
- This event was likely caused by the Northwest Pacific anomalous anticyclone (AAC) and La Niña-induced Walker circulation intensification
- Increasing 2020-like rainfall extremes are projected due to increase in future atmospheric water vapor and AAC frequency

Supporting Information:

Supporting Information may be found in the online version of this article.

Correspondence to:




K. Hu and G. Huang,
hkm@mail.iap.ac.cn;
hg@mail.iap.ac.cn

Citation:

Tang, H., Wang, J., Hu, K., Huang, G., Chowdary, J. S., Wang, Y., et al. (2022). Increasing 2020-like boreal summer rainfall extremes over Northeast Indian subcontinent under greenhouse warming. *Geophysical Research Letters*, 49, e2021GL096377. <https://doi.org/10.1029/2021GL096377>

Received 28 SEP 2021
Accepted 15 MAY 2022

Increasing 2020-Like Boreal Summer Rainfall Extremes Over Northeast Indian Subcontinent Under Greenhouse Warming

Haosu Tang^{1,2} , Jun Wang¹ , Kaiming Hu¹ , Gang Huang^{1,2} , Jasti S. Chowdary³ , Ya Wang^{1,2} , Ziyue Wang⁴, and Bin Tang^{1,2}

¹State Key Laboratory of Numerical Modeling for Atmospheric Sciences and Geophysical Fluid Dynamics (LASG)/Key Laboratory of Regional Climate Environment for Temperate East Asia (RCE-TEA)/Center for Monsoon System Research (CMSR), Institute of Atmospheric Physics, Chinese Academy of Sciences, Beijing, China, ²University of Chinese Academy of Sciences, Beijing, China, ³Indian Institute of Tropical Meteorology, Ministry of Earth Sciences, Pune, India, ⁴Key Laboratory of Meteorological Disaster, Ministry of Education / Joint International Research Laboratory of Climate and Environmental Change/Collaborative Innovation Center on Forecast and Evaluation of Meteorological Disasters, Nanjing University of Information Science and Technology, Nanjing, China

Abstract Extreme persistent rainfall poses serious impacts on human and natural systems, predominately through its related hydrogeological disasters. Due to sustained heavy downpours, the summer of 2020 was the second wettest on record over Northeast Indian subcontinent since 1901. Here, we find that this orographically anchored extreme rainfall event was largely associated with the anomalous anticyclone (AAC) over the Indo-Northwest Pacific region and La Niña-induced Walker circulation intensification. The overall effect of anthropogenic forcings contributed little to the occurrence probability of this event, because the warming and wetting effects of greenhouse gases were almost negated by anthropogenic aerosols. Climate models project a prominent increasing trend of such extreme event under future greenhouse-induced warming due to increase in atmospheric water vapor and 2020-like AAC frequency. Our findings thus call for scaling up climate change adaptation efforts for increasingly extreme persistent rainfall in highly populated but low-resilience South Asian developing countries.

Plain Language Summary Due to windward slope topography and monsoon activities, the populated Northeast Indian subcontinent (NEI) suffers from heavy rainfall and floods almost every year. Extreme persistent downpours lashed NEI in summer 2020, ranked the second heaviest on record since 1901. This event caused about 550 fatalities and economic loss up to hundreds of millions of dollars. It is highly compelling but challenging to understand the weather drivers and future risks of this high-impact event. Here, we suggested this event was likely caused by the anomalous anticyclone (AAC) over the Indo-Northwest Pacific region and La Niña-induced Walker circulation intensification. The overall effect of current human-induced climate change contributed little to the occurrence probability of this event, as most of the warming and wetting effects of greenhouse gases were canceled out by anthropogenic aerosols. Climate models project an increasing risk of 1.77 (1.97), 2.08 (2.59), 2.58 (3.88), and 3.10 (5.52) times of such extreme event in the median-term (long-term) future under *SSP1-2.6*, *SSP2-4.5*, *SSP3-7.0*, and *SSP5-8.5*, respectively. It is mainly caused by the increases in atmospheric water vapor and 2020-like AAC frequency. Our findings indicate that future flooding risk over NEI will increase robustly if greenhouse warming continues.

1. Introduction

During early summer (mid-June to late-July) 2020, unprecedented persistent rainfall and flooding hit large parts of Asia, including south-central and eastern China, as well as western Japan, and affected millions of people (WMO News, 2020). An equally destructive but barely studied event was rainfall extremes occurring over the Northeast Indian subcontinent (NEI; 25–28°N, 84–97°E; red box in Figure 1b). This persistent heavy rainfall event (hereafter termed 2020 event) caused multiple hydrogeological disasters across Northeast India and neighboring South Asian countries. As much as a third of Bangladesh was inundated by the devastating floods induced by this extreme event. This disastrous event was reported to leave ~550 people dead or missing and 9.6 million people affected, resulting in the direct economic loss up to hundreds of millions of dollars (IFRC News, 2020).

During June–July (JJ) 2020, the tropical anomalous sea surface temperature (SST) pattern mainly featured warming in the Indian Ocean and cooling in the equatorial eastern Pacific (Figure 1a). This concurrent Indo-Pacific

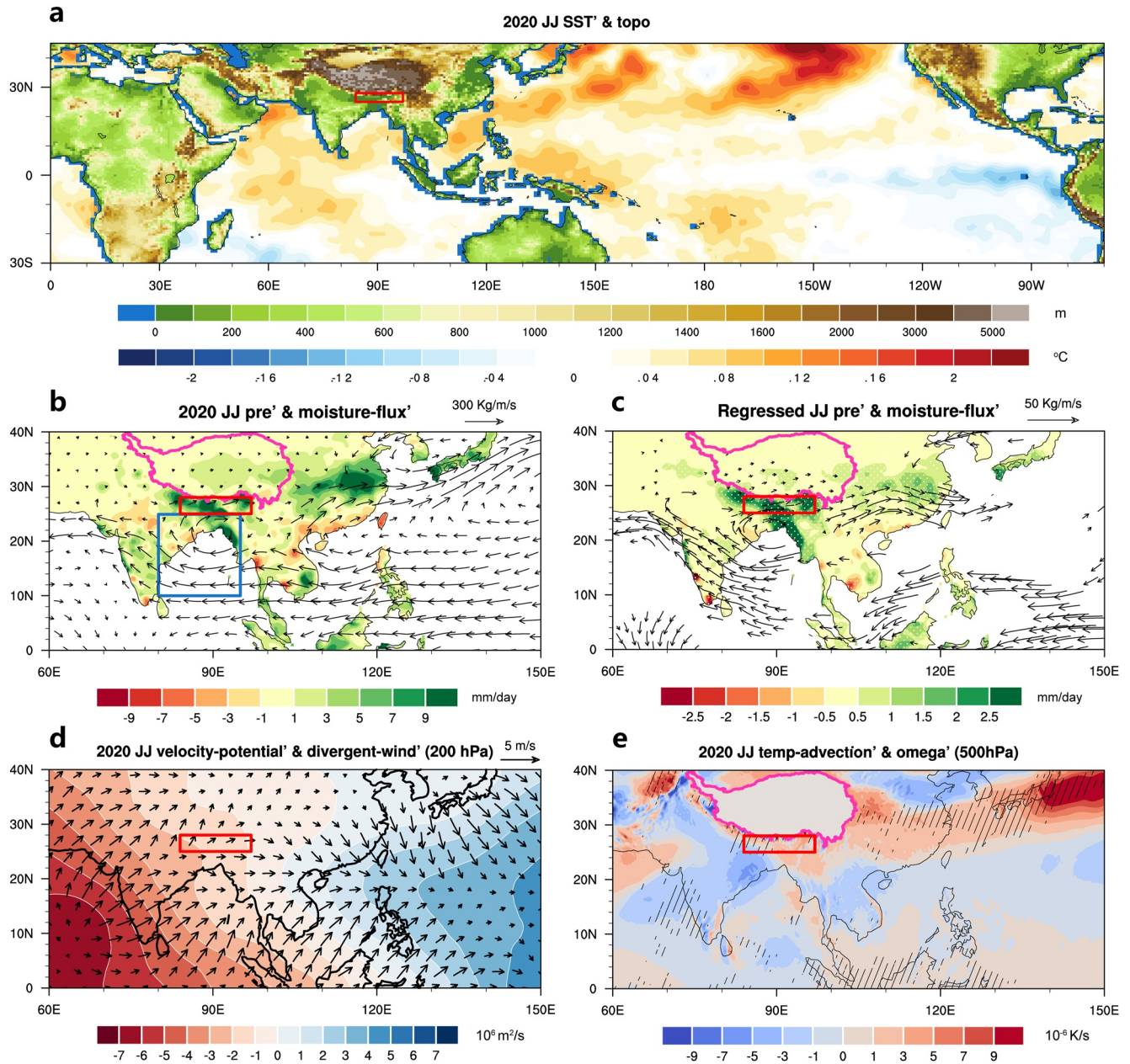


Figure 1. (a) Sea surface temperature (SST) anomalies (colors; K) in June–July (JJ) 2020 and elevation (colors; m). Red box marks the Northeast Indian subcontinent (NEI) (25°–28°N, 84°–97°E). (b) Rainfall anomalies (colors; mm/day) and vertically integrated moisture flux anomalies (vectors; $\text{kg} \cdot \text{m}^{-1} \cdot \text{s}^{-1}$) in JJ 2020. Blue box marks the Bay of Bengal (10°–25°N, 80°–95°E). The Tibetan Plateau is highlighted in pink curve. (c) Regression of rainfall anomalies (colors; mm/day) and vertically integrated moisture flux anomalies (vectors; $\text{kg} \cdot \text{m}^{-1} \cdot \text{s}^{-1}$) onto the JJ mean rainfall averaged over NEI from 1991 to 2020. Vectors only exceeding the 90% confidence level are shown and white dots indicate the statistically significant anomalies at the 0.1 significance level. (d) Potential velocity anomalies (colors; $\times 10^6 \text{ m}^2 \cdot \text{s}^{-1}$) and relevant divergent wind component anomalies (vectors; $\text{m} \cdot \text{s}^{-1}$) at 200 hPa in JJ 2020. (e) Same as (d), but for temperature advection (colors; $\times 10^{-6} \text{ K} \cdot \text{s}^{-1}$) and omega anomalies (hatched, only $< -0.03 \text{ Pa} \cdot \text{s}^{-1}$ are shown) at 500 hPa. The Tibetan Plateau has been masked out before plotting.

tropical anomalous SST boundary condition plus the long-lasting Madden-Julian Oscillation active phase over the Indian Ocean favored the formation and maintenance of Northwest Pacific (NWP) anomalous anticyclone (AAC) (Takaya et al., 2020; W.; Zhang, Huang, et al., 2021; Zhou et al., 2021). The southeasterlies of AAC intensified the anomalous moisture transport from tropical oceans, thereby persistent intense rainfall over East Asia as documented by numerous literatures (e.g., Cai et al., 2022; Hu et al., 2017; Liang et al., 2021; Tang et al., 2022; L. Zhang, Zhao, et al., 2021).

Previous studies suggested that AAC could modulate the South Asian summer monsoon (SASM) rainfall on the interannual timescale during El Niño-Southern Oscillation (ENSO) decaying summer (e.g., Chowdary et al., 2013, 2019; Darshana et al., 2020; Kosaka, 2021; Xie et al., 2016; Zhou, Zhang, & Xie, 2019; Zhou, Xie, & Zhang, 2019). The anomalous low-level moisture convergence brought by the AAC and orographic lifting over the southern slope of East Himalayas may induce heavy rainfall in Bangladesh and Assam region during El Niño decaying summer. In addition, ENSO is well recognized to directly influence the interannual variability of the SASM (e.g., Rasmusson & Carpenter, 1983; Yang & Huang, 2021). The SASM rainfall tends to decrease (increase) during El Niño (La Niña) developing summer through suppressed (intensified) Walker circulation (Walker, 1924).

Over the past decade, emerging evidences suggest that anthropogenic climate change is responsible for the observed increasing and intensifying rainfall extremes globally (e.g., IPCC, 2021; Min et al., 2011; Mukherjee et al., 2018; Singh et al., 2019), but the human influences on individual extreme events entail further quantification. Several attribution studies have been conducted on the extreme rainfall cases occurring in the Indian subcontinent, their results, however, are not qualitatively consistent. Some studies found an increased occurrence probability of extreme monthly or 6-day rainfalls due to anthropogenic forcing (Rimi et al., 2019; Singh et al., 2014), whereas others failed to detect significant anthropogenic influences on the risk of historical individual extreme 1-day or monthly rainfall cases (Philip et al., 2019; van Oldenborgh et al., 2016). This inconsistency may result from distinct features of rainfall events focused and varying attribution methods used. The biggest difference between the 2020 event and other previous extreme rainfall cases is that the 2020 event occurred at the start of monsoon season, which increased local water levels and made soil saturated, providing advantageous conditions for the ensuing extreme disasters like catastrophic floods and landslides during the following monsoon months.

In this study, we aim to understand the drivers and future risks of this high-impact event. The following questions need to be addressed: (a) was the 2020 event linked to internal variability of climate system? (b) what is the role of anthropogenic forcing? (c) will we experience more 2020-like rainfall extremes in the future? The rest of this paper is organized as follows. The data and methods are depicted in Section 2. The main results are presented in Section 3, followed by conclusion and discussion in Section 4.

2. Data and Methods

2.1. Data

We used the Climate Prediction Center (CPC) daily unified gauge-based rainfall data set from 1979 to 2020 on a $0.5^\circ \times 0.5^\circ$ grid (Xie et al., 2007). Considering that the temporal coverage of Climate Prediction Center (CPC) rainfall data set is too short for attribution analysis, we only used it to quantify the 2020 event preliminarily. From Figure 2 on, we employed the daily rainfall data set over 1901–2020 on a $0.25^\circ \times 0.25^\circ$ grid as the observations, which were produced by the India Meteorological Department (IMD) based on 6,995 Indian meteorological stations (Pai et al., 2014; Rajeevan et al., 2008). We used the fifth generation European Center for Medium-Range Weather Forecasts reanalysis (ERA5; Hersbach et al., 2020) to calculate the monthly mean three-dimensional winds, air temperature, sea level pressure (SLP) and vertical integral of moisture fluxes over 1979–2020. The ERA5 reanalysis product has 37 vertical levels from 1000 hPa to 1 hPa with a horizontal resolution of 0.25° . We also used the Met Office Hadley Center monthly SST data set on a global 1° grid (Rayner et al., 2003). All the anomalies in 2020 were calculated relative to the climate normal over 1981–2010.

We probed the role that anthropogenic forcing has played in the occurrence probability of the 2020 event mainly through the HadGEM3-GA6-based attribution system (Ciavarella et al., 2018). HadGEM3-GA6 is a global atmospheric general circulation model with daily temporal resolution and the highest spatial resolution in current attribution studies (85 vertical levels and $0.56^\circ \times 0.83^\circ$ horizontal resolution). Three sets of ensemble simulations were incorporated (Christidis et al., 2013):

1. The historical ensemble, forced by realistic SST and both natural (solar activities plus volcanic aerosols) and anthropogenic forcings, comprises 15 members for 1960–2013 with varying initial conditions (termed *Historical*).
2. The 2020 ensembles include 525 members of "actual" simulations forced by realistic 2020 SST and natural plus anthropogenic forcings (termed *HisExt-2020*), and 525 members of "counterfactual" simulations forced

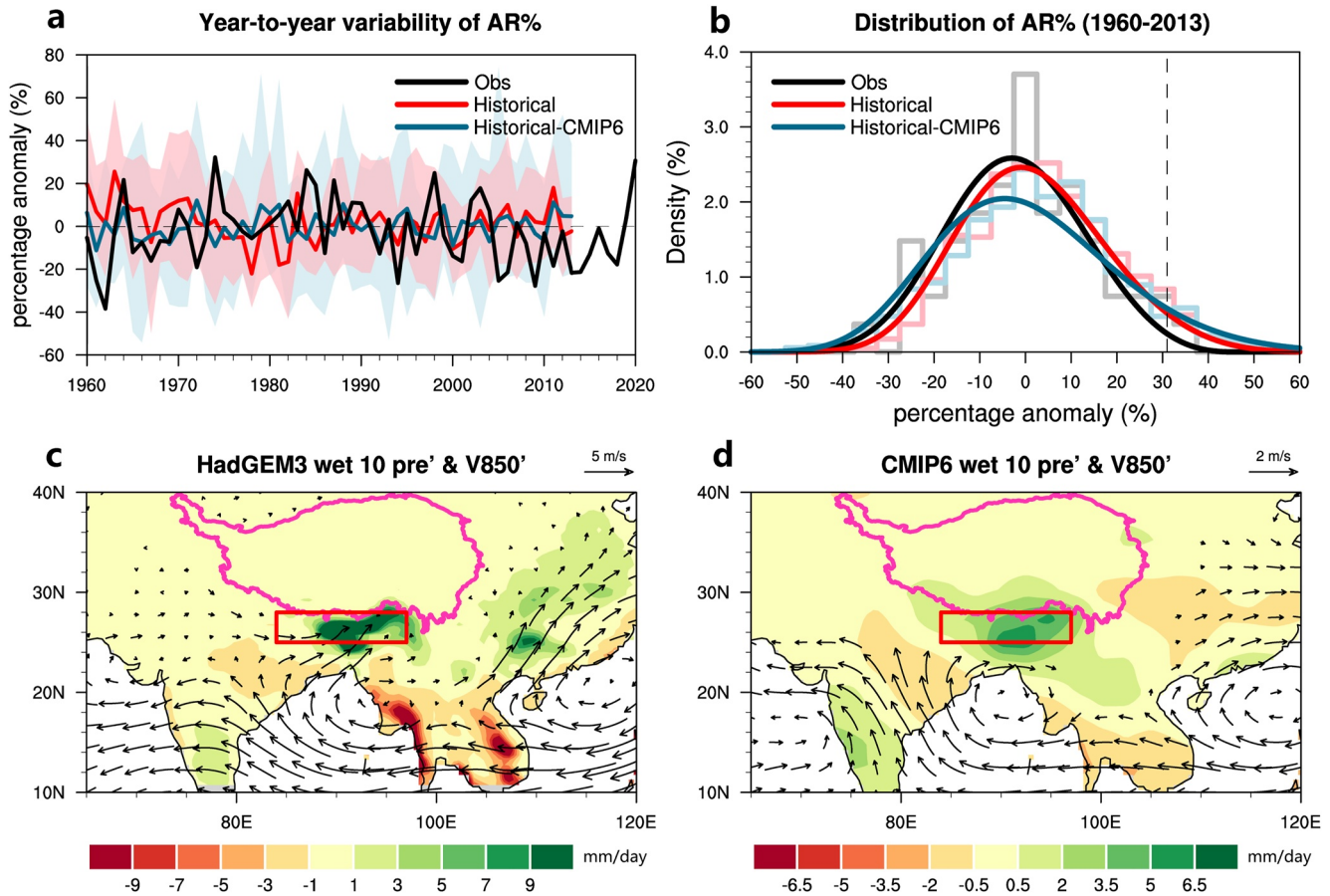


Figure 2. (a) Time series of accumulated rainfall (AR%) for the observations (black), *Historical* (red), and *Historical-CMIP6* (blue). The red and blue shadings indicate the ensemble spread of *Historical* and *Historical-CMIP6*, respectively. The solid lines denote their ensemble means. (b) Generalized extreme value-fitted probability density functions (solid lines) and raw histograms (translucent lines) of AR% for the observations (black), *Historical* (red), and *Historical-CMIP6* (blue) for 1960–2013. The dashed black line indicates the threshold of the observed 2020 event. (c) The composite JJ mean rainfall anomalies (colors; mm/day) and 850 hPa wind anomalies (vectors; $\text{m} \cdot \text{s}^{-1}$) averaged by the 10 members with the wettest AR% in *Historical* for 1960–2013. Rainfall anomalies in the oceans are masked out. (d) Same as (c), but for *Historical-CMIP6*.

by natural forcing only and observed 2020 SST but with human influences removed (termed *HisNatExt-2020*). The *Historical* ensemble was used to evaluate the HadGEM3-GA6, and the two 2020 ensembles were used for attribution.

To further verify the HadGEM3-GA6-based attribution results and project future 2020-like rainfall extremes, seven ensemble daily datasets from 13 models participating in the CMIP6 Detection and Attribution Model Intercomparison Project (Table S1 in Supporting Information S1; Eyring et al., 2016; Gillett et al., 2016) were analyzed. Because the ensemble sizes of different models are not same, only the first member of each model in each ensemble was selected.

1. The historical ensembles were forced by natural plus anthropogenic forcings (termed *Historical-CMIP6*) and hisNat ensembles forced by natural-only forcings (termed *HisNat-CMIP6*). Considering that the ocean states in these coupled models are evolving and not in line with realistic boundary conditions, we selected the period of 1995–2014 to denote the present climate backgrounds in CMIP6 simulations. Selecting this period also minimizes the potential influences of major volcano eruptions like the Pinatubo eruption in 1991.
2. The hisGHG and hisAer ensembles were used to disentangle the individual roles of greenhouse gases (GHG) and anthropogenic aerosols (termed *HisGHG-CMIP6* and *HisAer-CMIP6*, respectively).
3. Future projections under four tier-1 Shared Socioeconomic Pathways (*SSP1-2.6*, *SSP2-4.5*, *SSP3-7.0*, and *SSP5-8.5*; O'Neill et al., 2016) were analyzed to examine the changes in the occurrence probability of 2020-like

rainfall extremes during three future time periods (short-term: 2021–2040, median-term: 2051–2070, and long-term: 2081–2100). The *SSP3-7.0* includes 12 models since HadGEM3-GC31-LL did not carry out future projection for this scenario.

2.2. Methods

The JJ accumulated rainfall (AR) averaged over NEI was used to depict the 2020 event. In addition, the regional-mean maximum 28-day rainfall accumulations (RX28d) during boreal summer (June–August, JJA) was calculated to test the robustness of attribution result against different rainfall indices. We extended the time period to JJA mainly considering the models might not simulate SASM punctually with sophisticated topography over NEI and multi-scale feedback processes inherent in the SASM system. Both indices were normalized to anomaly percentages (termed AR% and RX28d%) relative to the climate normal (1981–2010) to rectify the model climatology biases.

The generalized extreme value (GEV) distribution (Jenkinson, 1955) was used to fit the probability density function (PDF) of rainfall indices, and the two-sample Kolmogorov–Smirnov (K–S) test was applied to test the GEV goodness-of-fit (Wilks, 2006). To quantitatively assess human contribution to the 2020 event, the probability ratio (PR, defined as $P_{\text{ALL}}/P_{\text{NAT}}$) based on GEV fit was computed. Here, P_{ALL} (P_{NAT}) denotes the exceedance probability of the 2020 event in the GEV-fitted distributions of All- (Natural-only) forced runs. The uncertainty of PR was estimated via bootstrapping (Efron & Tibshirani, 1994), that is, resampling ensemble members 1,000 times. The total uncertainty (5–95th percentile range) was derived from 1,000,000 combinations of P_{ALL} and P_{NAT} .

The AR% and RX28d% were first calculated on their original grids and then bilinearly interpolated to a common 1° grid. Other interpolation techniques (i.e., bicubic and inverse distance weighted interpolation) were further applied for validation and similar results were obtained (not shown). The AAC index was defined as JJA mean SLP averaged over the Bay of Bengal (10°–25°N, 80°–95°E; blue box in Figure 1b). The two-tailed student's *t* test was used to test the statistical significance of linear regression and composite analyses.

3. Results

3.1. The Drivers Behind the 2020 Event

During JJ 2020, the AAC spanning across the Indo-NWP region strengthened moisture transport from the warm Bay of Bengal to NEI continuously, and thus led to extreme persistent rainfall via local orographic lifting (Figure 1b). Besides, an intensified AAC was generally associated with increased NEI rainfall in the historical period ($r = 0.45$, $p < 0.01$, $n = 42$), and both of them showed a record high in the year 2020 (Figure S1 in Supporting Information S1). The patterns of regressed rainfall and vertically integrated moisture flux anomalies onto the JJ mean rainfall averaged over NEI during 1991–2020 bear notable similarities to the observed ones in JJ 2020. The AAC extends to South Asia, decreasing the rainfall over the Indian monsoon trough region but increasing the rainfall in the south of East Himalayas (Figure 1c; Chowdary et al., 2019). The time period of 1991–2020 was selected because the AAC is stronger and more westward-extended after the mid-1980s (Hu et al., 2020), resulting in enhanced impacts on NEI.

In addition to the reinforced moisture transport, the Indian Ocean warming and developing La Niña in JJ 2020 caused an intensified Walker circulation, which led to much stronger upward motion over NEI (Figure 1d). Moreover, the upper-level anomalous warm air advection from the climatological warm Tibetan Plateau to cold NEI forced adiabatic updraft as well (Figure 1e; Chowdary et al., 2021). The warm air advections can be further traced to the intensified mid-tropospheric westerly jet induced by the Indian Ocean warming (Qu & Huang, 2011; Zhou et al., 2021).

The relatively short temporal coverage (1979–2020) and potential biases of the Climate Prediction Center (CPC) rainfall data set hinder further understanding of the long-term rainfall variability over NEI. To overcome this, we used the IMD daily rainfall data set (1901–2020) as a proxy to delineate the rainfall variability over NEI, since most areas of it are covered by India. The interannual variabilities of NEI JJ mean rainfall show consistencies between two datasets for the period of 1979–2020 ($r = 0.52$, $p < 0.01$, $n = 42$). In addition, both datasets exhibit much more rainfall in JJ 2020 (Figure S2 in Supporting Information S1). The 2020 event is mainly concentrated from mid-June to late July, with several rounds of daily rainfall extremes (Figure S3a in Supporting

Information S1). The AR% is 31% above the 1981–2010 climatological counterparts, which ranks the second heaviest rainfall event (weaker than the 1974 event) in the reliable observations since 1901 and corresponds to an approximate 1-in-60-year event (Figure S3b in Supporting Information S1). The RX28 d% is 32% above the 1981–2010 climatology, which is the most extreme one on the century-long record (not shown).

3.2. Evaluation of the Models

We first evaluated the performances of the HadGEM3-GA6 and CMIP6 simulations in depicting NEI rainfall statistical characteristics. The HadGEM3-GA6 and CMIP6 models can reproduce year-to-year variability of AR%, as the observed time series is generally enveloped within the uncertainty bounds of the model simulations (Figure 2a). In addition, the PDFs of the observed and stimulated AR% cannot be distinguished by the K–S test at the 0.05 significance level (Figure 2b, $p = 0.25$ for HadGEM3-GA6 and $p = 0.40$ for the whole CMIP6 models; see Table S1 in Supporting Information S1 for values of each CMIP6 model). Evaluation results are similar for RX28 d% ($p = 0.29$ for HadGEM3-GA6 and $p = 0.25$ for the whole CMIP6 models). The large-scale anomalous atmospheric circulations resulting in the rainfall extremes over NEI were extracted from the HadGEM3-GA6 and CMIP6 simulations, by picking out 10 members with the wettest AR% in *Historical* and *Historical-CMIP6*, respectively (Figures 2c and 2d). The westward-extended AACs in both simulations highly resemble the observations, lending confidence to the following attribution study.

3.3. Anthropogenic Influence on the 2020 Event

The PDFs of AR% derived from *HisExt-2020* and *HisNatExt-2020* were compared to probe the anthropogenic influences on the 2020 event. There is an overall shift of PDF towards drier scenario, while its right tail becomes larger from *HisNatExt-2020* to *HisExt-2020*. It connotes that anthropogenic forcings act to decrease total rainfall but increase the occurrence probability of the 2020-like rainfall extremes from 8‰ (4–12‰) for P_{NAT} to 13‰ (6–19‰) for P_{ALL} (Figure 3a). Correspondingly, the return period of the 2020 event tends to be shorter in the actual climate (~1-in-80-year) in comparison to the "natural" world (~1-in-130-year; Figure 3b). However, the 90% uncertainty interval of PR estimates for AR% (1.64, 0.67–3.64) encompasses the unity, indicating the above conclusion is not statistically robust for the present-day climate. The estimate of PR for RX28d% (1.36, 0.73–3.03) is inconclusive as well (Figures S4a and S4b in Supporting Information S1). As for the CMIP6 simulations, the PDFs overall drying shift from *HisNat-CMIP6* to *Historical-CMIP6* is consistent with the HadGEM3-GA6 results, whereas a larger right tail is not apparent for *Historical-CMIP6* compared to *HisNat-CMIP6*. A PR of 0.85 (0.50–1.30) is estimated for AR% (Figure 3c) and a PR of 0.79 (0.38–1.15) for RX28d% based on CMIP6 simulations (Figure S4c in Supporting Information S1). Therefore, it can be concluded that no statistically significant anthropogenic influence could be detected in the occurrence probability of 2020 event for the current level of climate change.

To deepen the understanding of above attribution results, the anthropogenic forcings in CMIP6 models were decomposed into two dominant parts, that is, anthropogenic GHG and aerosols. The PDF shifts towards drier scenario from *Historical-CMIP6* to *HisAer-CMIP6*, but moves towards wetter for *HisGHG-CMIP6* (Figure 3d). Given relatively small influences of natural forcing and large-scale land use changes, the difference between *Historical-CMIP6* and *HisAer-CMIP6* (*HisGHG-CMIP6*) can be largely attributed to the effect of GHG (aerosols). This means that historical GHG emission increased the occurrence probability of 2020-like rainfall extremes by 1.6 (1.0–2.5) times. On the other hand, the historical anthropogenic aerosols reduced the event probability by 55% (37%–75%). Similar conclusions could be obtained for RX28 d% (Figure S4d in Supporting Information S1). In other words, the boosting effect of GHG on SASM was mostly canceled out by anthropogenic aerosols, leading to undetectable human influence on the 2020 event.

How to understand the contrasting effects of GHG and anthropogenic aerosols? Previous studies suggested that increased GHG warms the earth surface via greenhouse effect, increasing precipitable water in the atmosphere according to the Clausius–Clapeyron scaling relation (Figure S5a in Supporting Information S1; e.g., Ayan-tika et al., 2021; Hu et al., 2021; Lau & Kim, 2017; Li et al., 2015). The relevant mechanisms for aerosols are almost opposite to GHG. The aerosols overall act to diminish the solar radiation reaching the surface, inducing surface cooling and less atmospheric precipitable water (Figure S5b in Supporting Information S1; e.g., Bollasina et al., 2011; Krishnan et al., 2015). Moreover, the diminished surface temperature gradient between NEI and

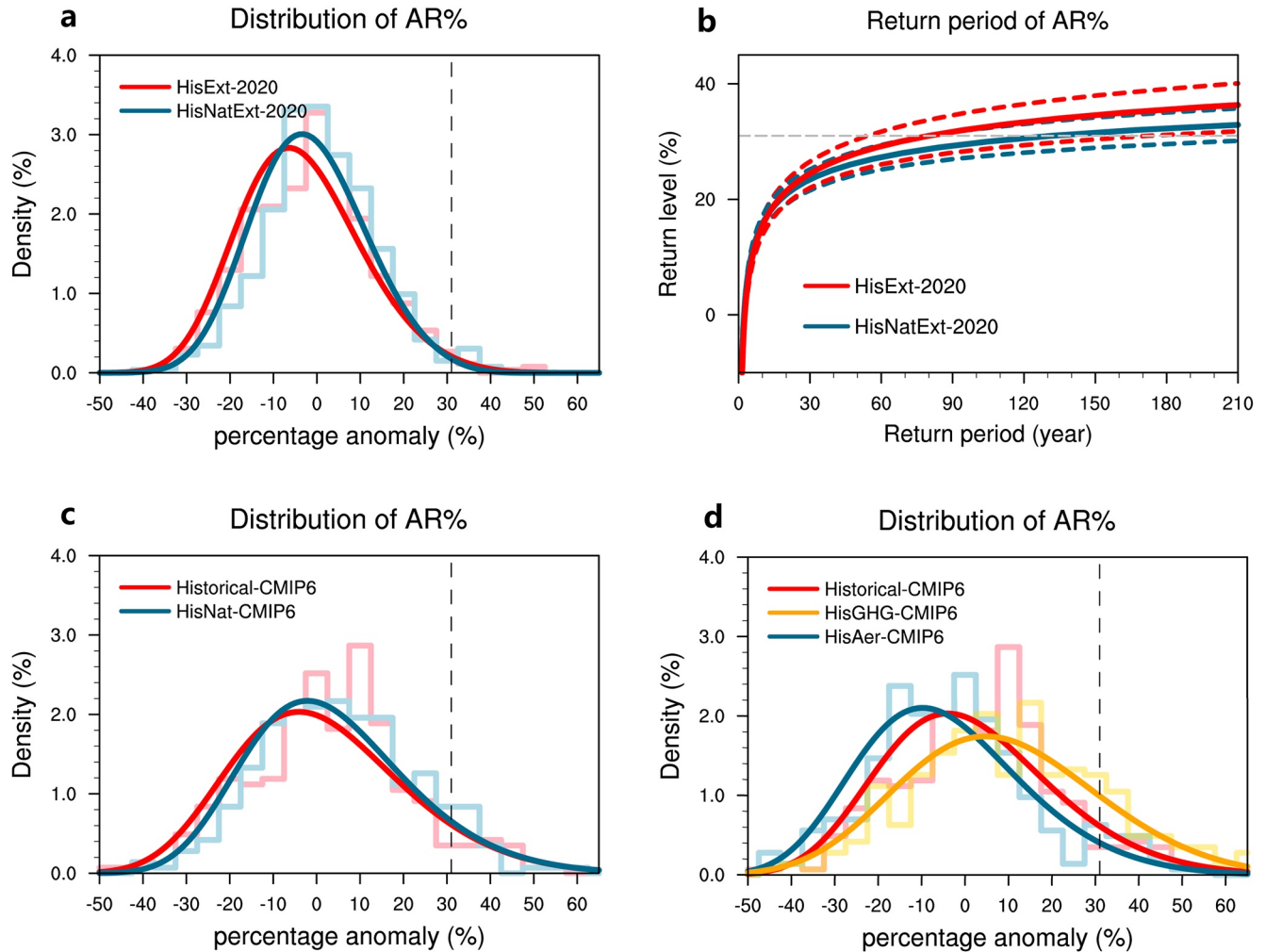


Figure 3. (a) Generalized extreme value-fitted probability density functions (solid lines) and raw histograms (translucent lines) of accumulated rainfall (AR)% for *HisExt-2020* (red) and *HisNatExt-2020* (blue). The dashed black line indicates the threshold of the observed 2020 event. (b) The return periods (solid lines) of AR% for *HisExt-2020* (red) and *HisNatExt-2020* (blue). The corresponding 5%–95% uncertainty ranges (dashed lines) are shown. The dashed gray line indicates the threshold of the observed 2020 event. (c) Same as (a), but for *Historical-CMIP6* (red) and *HisNat-CMIP6* (blue) for 1995–2014. (d) Same as (a), but for *Historical-CMIP6* (red), *HisGHG-CMIP6* (yellow) and *HisAer-CMIP6* (blue) for 1995–2014.

tropical oceans in boreal summer could further weaken the monsoon Hadley circulation, thereby attenuating the SASM (Ramanathan et al., 2005).

3.4. Future Projections

Although anthropogenic influence on the 2020 event for the present-day climate is inconclusive, future projections under various emission scenarios may be of more confidence, since the emissions of anthropogenic aerosols and their precursors in Asia tend to decline while the GHG will rise steadily in the future. In that case, the weakened aerosol effects plus the enhanced GHG effects will elevate the occurrence probability of 2020-like rainfall extremes in the future, as predicted by CMIP6 models (Figure 4a; with AR% as the rainfall index). In the short-term future, the occurrence probability of 2020-like rainfall extremes will slightly increase by ~ 1.5 -fold under all emission scenarios. However, ongoing global warming will increase the probability by 1.77 (1.97), 2.08 (2.59), 2.58 (3.88), and 3.10 (5.52) times in the median-term (long-term) future under *SSP1-2.6*, *SSP2-4.5*, *SSP3-7.0*, and *SSP5-8.5*, respectively (Figure 4b). Similar results could be obtained for RX28d% (Figure S6 in Supporting Information S1).

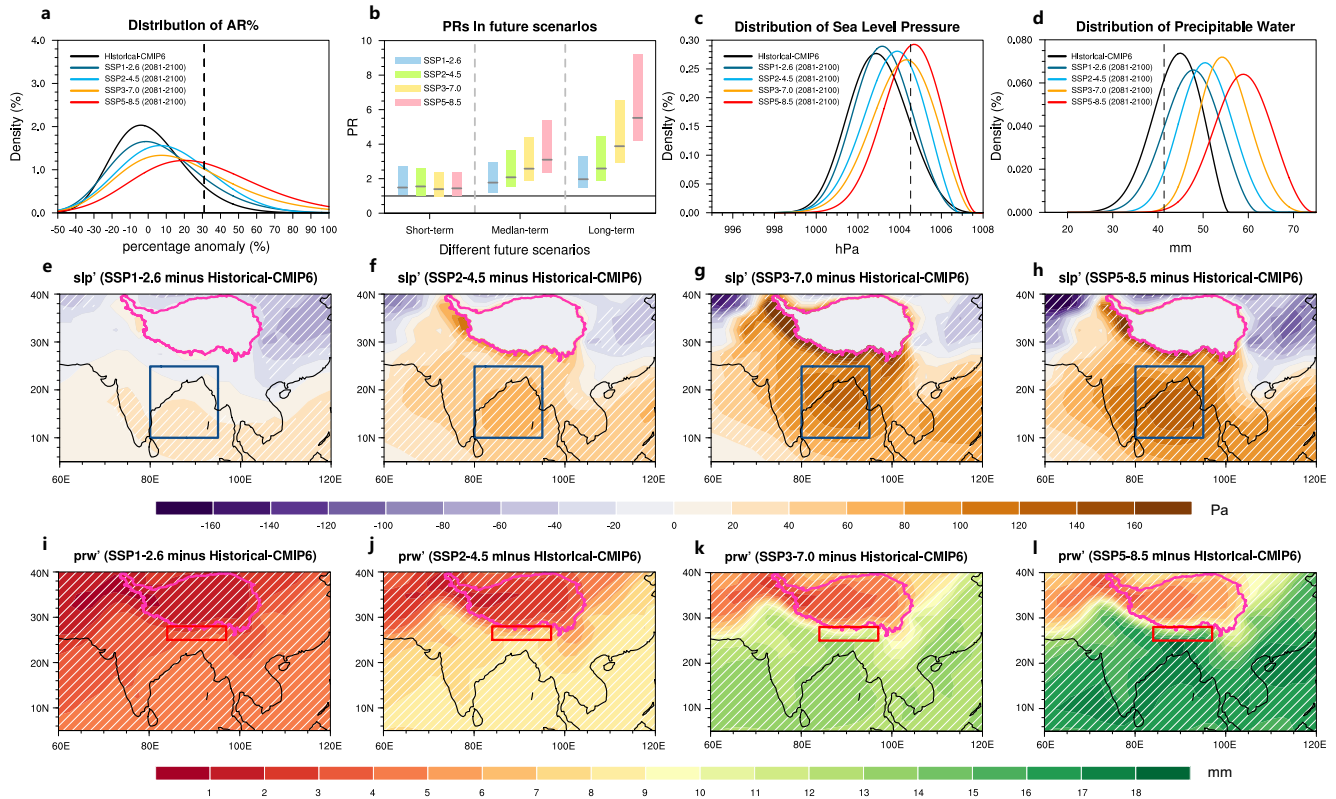


Figure 4. (a) Generalized extreme value-fitted probability density functions (solid lines) of accumulated rainfall (AR%) in *Historical-CMIP6* (black) for 1995–2014, and Shared Socioeconomic Pathways (*SSP1-2.6*) (dark blue), *SSP2-4.5* (light blue), *SSP3-7.0* (orange), *SSP5-8.5* (red) for 2081–2100. The dashed black line indicates the observed threshold of 2020 event. (b) PRs (gray lines) of AR% for the short-term (2021–2040), median-term (2051–2070), and long-term (2081–2100) projection periods under *SSP1-2.6* (blue), *SSP2-4.5* (green), *SSP3-7.0* (yellow) and *SSP5-8.5* (pink) scenarios. The bars denote the 5%–95% uncertainty range of PRs. The gray solid line denotes where PR equals 1. (c) Same as (a), but for June–August (JJA) mean sea level pressure (SLP) averaged over the Bay of Bengal (10–25°N, 80–95°E; blue box). (d) Same as (a), but for JJA mean precipitable water averaged over Northeast Indian subcontinent (25°–28°N, 84°–97°E; red box). (e–h) Ensemble mean differences of JJA mean SLP (colors; Pa) between *SSP1-2.6*, *SSP2-4.5*, *SSP3-7.0*, *SSP5-8.5* (2081–2100) and *Historical-CMIP6* (1995–2014), respectively. Hatched areas denote the differences are statistically significant at 0.1 significance level. The Tibetan Plateau has been masked out before plotting. (i–l) Same as (e–h), but for JJA mean precipitable water (colors; mm). The Tibetan Plateau is highlighted in pink curve.

To improve the physical understanding of future projection results, we further investigated the roles of human-induced dynamic and thermodynamic changes. The PDF of AAC magnitude shifts rightward from *Historical-CMIP6* to *SSP5-8.5* (Figure 4c), indicating the 2020-like high-pressure system over the Bay of Bengal would be more likely to appear under greenhouse warming (Figures 4e–4h). As a result, increasing 2020-like rainfall extremes may be on the way. In addition, the PDF of JJA mean precipitable water averaged over NEI shifts rightward from *Historical-CMIP6* to *SSP5-8.5* (Figure 4d), in line with the classic "wet-get-wetter" paradigm (Held & Soden, 2006). The anthropogenically driven increase in atmospheric precipitable water provides more ammunition for future 2020-like precipitation extremes (Figures 4i–4l). Therefore, when 2020-like AAC emerges over the Indo-NWP region in the future, even of the same magnitude as today, the NEI might experience substantially intensified rainfall due to anthropogenically-driven thermodynamic changes.

4. Conclusion and Discussion

The 2020 summer extreme rainfall over NEI was the second wettest on record since 1901, and wreaked havoc on the densely populated South Asian developing countries. In this study, we investigated the driver of this event and, by extension, its projections under greenhouse warming. Two storylines were unfolded in the present study:

1. From the perspective of natural variability, our study suggested that the 2020 event was likely caused by the AAC over the Indo-NWP region and La Niña-related Walker circulation intensification. Increase in 2020-like AAC frequency may bring more boreal summer rainfall extremes over NEI in the future.

2. From the view of extreme event attribution, we found that the effects of GHG and anthropogenic aerosols on the occurrence probability of 2020 event were opposite. The GHG-induced warming increased the probability, which was negated by the effect of anthropogenic aerosols. This led to undistinguished role of anthropogenic forcings in the 2020 event. However, the results for the present-day climate cannot infer the future, given the Asian anthropogenic aerosol emissions are expected to decline while the GHG rise steadily. In that case, the weakened aerosol effects plus the enhanced GHG effects (thus more atmospheric water vapor) may potentially increase the probabilities of 2020-like events over NEI in the future.

The limitations stemming from the spatiotemporal brevity of the observational records, the skills of current climate models and the physical understanding of processes behind the extreme events inevitably bring uncertainties to the extreme event attribution. Therefore, high-quality observations and models are required in future event attribution studies, and the attribution methods should undergo continuous improvement as well. Another limitation of this study is that our model simulations did not consider the COVID-induced aerosol reductions in 2020, which was suggested beneficial for the hydrological cycle over South Asia (Fadnavis et al., 2021). To what extent did COVID-induced anthropogenic forcing changes affect on the 2020 event deserves further study.

Data Availability Statement

CMIP6 datasets could be downloaded from <https://esgf-node.llnl.gov/search/cmip6/> (see details in Table S1 in Supporting Information S1). Climate Prediction Center rainfall data set is located at <https://psl.noaa.gov/data/gridded/data.cpc.globalprecip.html>. India Meteorological Department rainfall data set is located at https://cdsp.imdpune.gov.in/home_gridded_data.php. ERA5 datasets could be accessed from <https://doi.org/10.24381/cds.6860a573>. HadISST data set could be accessed from <https://www.metoffice.gov.uk/hadobs/hadisst/>. HadGEM3-GA6 datasets are provided by DOI: <https://doi.org/10.1016/j.wace.2018.03.003> (Ciavarella et al., 2018).

Acknowledgments

This work is supported by the Strategic Priority Research Program of Chinese Academy of Sciences (XDA20060500), the National Natural Science Foundation of China (41831175, 42175040, 41775086), the Second Tibetan Plateau Scientific Expedition and Research (STEP) program (2019QZKK0102), and the Youth Innovation Promotion Association of CAS (2021072).

References

- Ayantika, D. C., Krishnan, R., Singh, M., Swapna, P., Sandeep, N., Prajeesh, A. G., & Vellore, R. (2021). Understanding the combined effects of global warming and anthropogenic aerosol forcing on the South Asian monsoon. *Climate Dynamics*, 56(5–6), 1643–1662. <https://doi.org/10.1007/s00382-020-05551-5>
- Bollasina, M. A., Ming, Y., & Ramaswamy, V. (2011). Anthropogenic aerosols and the weakening of the South Asian summer monsoon. *Science*, 334(6055), 502–505. <https://doi.org/10.1126/science.1204994>
- Cai, Y., Chen, Z., & Du, Y. (2022). The role of Indian Ocean warming on extreme rainfall in central China during early summer 2020: Without significant El Niño influence. *Climate Dynamics*. <https://doi.org/10.1007/s00382-022-06165-9>
- Chowdary, J. S., Gnanaseelan, C., & Chakravorty, S. (2013). Impact of Northwest Pacific anticyclone on the Indian summer monsoon region. *Theoretical and Applied Climatology*, 113(1–2), 329–336. <https://doi.org/10.1007/s00704-012-0785-9>
- Chowdary, J. S., Patekar, D. D., Srinivas, G., Gnanaseelan, C., & Parekh, A. (2019). Impact of the Indo-Western Pacific Ocean capacitor mode on South Asian summer monsoon rainfall. *Climate Dynamics*, 53(3–4), 2327–2338. <https://doi.org/10.1007/s00382-019-04850-w>
- Chowdary, S., Vibhute, A. S., Darshana, P., Parekh, A., Gnanaseelan, C., & Attada, R. (2021). Meridional displacement of the Asian jet and its impact on Indian summer monsoon rainfall in observations and CFSv2 hindcast. *Climate Dynamics*, 58(3–4), 811–829. <https://doi.org/10.1007/s00382-021-05935-1>
- Christidis, N., Stott, P. A., Scaife, A. A., Arribas, A., Jones, G. S., Copsey, D., et al. (2013). A new HadGEM3-A-based system for attribution of weather- and climate-related extreme events. *Journal of Climate*, 26(9), 2756–2783. <https://doi.org/10.1175/jcli-d-12-00169.1>
- Ciavarella, A., Christidis, N., Andrews, M., Groenendijk, M., Rostron, J., Elkington, M., et al. (2018). Upgrade of the HadGEM3-A based attribution system to high resolution and a new validation framework for probabilistic event attribution. *Weather and Climate Extremes*, 20, 9–32. <https://doi.org/10.1016/j.wace.2018.03.003>
- Darshana, P., Chowdary, J. S., Gnanaseelan, C., Parekh, A., & Srinivas, G. (2020). Interdecadal modulation of the Indo-Pacific Ocean capacitor mode and its influence on Indian summer monsoon rainfall. *Climate Dynamics*, 54(3–4), 1761–1777. <https://doi.org/10.1007/s00382-019-05085-5>
- Efron, B., & Tibshirani, R. J. (1994). *An introduction to the bootstrap*. CRC Press.
- Eyring, V., Bony, S., Meehl, G. A., Senior, C. A., Stevens, B., Stouffer, R. J., & Taylor, K. E. (2016). Overview of the Coupled Model Intercomparison Project Phase 6 (CMIP6) experimental design and organization. *Geoscientific Model Development*, 9(5), 1937–1958. <https://doi.org/10.5194/gmd-9-1937-2016>
- Fadnavis, S., Sabin, T. P., Rap, A., Müller, R., Kubin, A., & Heinold, B. (2021). The impact of COVID-19 lockdown measures on the Indian summer monsoon. *Environmental Research Letters*, 16(7), 074054. <https://doi.org/10.1088/1748-9326/ac109c>
- Gillett, N. P., Shiogama, H., Funke, B., Hegerl, G., Knutti, R., Matthes, K., et al. (2016). The detection and attribution model intercomparison project (DAMIP v1.0) contribution to CMIP6. *Geoscientific Model Development*, 9(10), 3685–3697. <https://doi.org/10.5194/gmd-9-3685-2016>
- Held, I. M., & Soden, B. J. (2006). Robust responses of the hydrological cycle to global warming. *Journal of Climate*, 19(21), 5686–5699. <https://doi.org/10.1175/jcli3990.1>
- Hersbach, H., Bell, B., Berrisford, P., Hirahara, S., Horányi, A., Muñoz-Sabater, J., et al. (2020). The ERA5 global reanalysis. *Quarterly Journal of the Royal Meteorological Society*, 146(730), 1999–2049. <https://doi.org/10.1002/qj.3803>

- Hu, K., Huang, G., Huang, P., Kosaka, Y., & Xie, S.-P. (2021). Intensification of El Niño-induced atmospheric anomalies under greenhouse warming. *Nature Geoscience*, 14(6), 377–382. <https://doi.org/10.1038/s41561-021-00730-3>
- Hu, K., Liu, Y., Huang, G., He, Z., & Long, S.-M. (2020). Contributions to the interannual summer rainfall variability in the mountainous area of central China. *Advances in Atmospheric Sciences*, 37(3), 259–268. <https://doi.org/10.1007/s00376-019-9099-5>
- Hu, K., Xie, S.-P., & Huang, G. (2017). Orographically anchored El Niño effect on summer rainfall in Central China. *Journal of Climate*, 30(24), 10037–10045. <https://doi.org/10.1175/jcli-d-17-0312.1>
- IFRC News. (2020). *South Asia floods: 9.6 million people swamped as humanitarian crisis deepens*. Retrieved from <https://reliefweb.int/report/bangladesh/south-asia-floods-96-million-people-swamped-humanitarian-crisis-deepens>. Accessed 27 September 2021.
- IPCC. (2021). *IPCC Sixth Assessment Report: Working Group I Report, "The Physical Science Basis"*. Cambridge University Press.
- Jenkinson, A. F. (1955). The frequency distribution of the annual maximum (or minimum) values of meteorological elements. *Quarterly Journal of the Royal Meteorological Society*, 81(348), 158–171. <https://doi.org/10.1002/qj.49708134804>
- Kosaka, Y. (2021). "Coupling of the Indian, western North Pacific, and east Asian summer monsoons", Chapter 13 of the book *Indian summer monsoon variability: ENSO teleconnections and beyond*. In J. S. Chowdary, A. Parekh, & C. Gnanaseelan (Eds.), Elsevier.
- Krishnan, R., Sabin, T. P., Vellore, R., Mujumdar, M., Sanjay, J., Goswami, B. N., et al. (2015). Deciphering the desiccation trend of the South Asian monsoon hydroclimate in a warming world. *Climate Dynamics*, 47(3–4), 1007–1027. <https://doi.org/10.1007/s00382-015-2886-5>
- Lau, W. K.-M., & Kim, K.-M. (2017). Competing influences of greenhouse warming and aerosols on Asian summer monsoon circulation and rainfall. *Asia-Pacific Journal of Atmospheric Sciences*, 53(2), 181–194. <https://doi.org/10.1007/s13143-017-0033-4>
- Li, X., Ting, M., Li, C., & Henderson, N. (2015). Mechanisms of Asian summer monsoon changes in response to anthropogenic forcing in CMIP5 models. *Journal of Climate*, 28(10), 4107–4125. <https://doi.org/10.1175/jcli-d-14-00559.1>
- Liang, P., Hu, Z.-Z., Ding, Y., & Qian, Q. (2021). The extreme Mei-yu Season in 2020: Role of the Madden-Julian oscillation and the cooperative influence of the Pacific and Indian oceans. *Advances in Atmospheric Sciences*, 38(12), 2040–2054. <https://doi.org/10.1007/s00376-021-1078-y>
- Min, S.-K., Zhang, X., Zwiers, F. W., & Hegerl, G. C. (2011). Human contribution to more-intense precipitation extremes. *Nature*, 470(7334), 378–381. <https://doi.org/10.1038/nature09763>
- Mukherjee, S., Aadhar, S., Stone, D., & Mishra, V. (2018). Increase in extreme precipitation events under anthropogenic warming in India. *Weather and Climate Extremes*, 20, 45–53. <https://doi.org/10.1016/j.wace.2018.03.005>
- O'Neill, B. C., Tebaldi, C., vanVuuren, D. P., Eyring, V., Friedlingstein, P., Hurtt, G., et al. (2016). The scenario model intercomparison project (ScenarioMIP) for CMIP6. *Geoscientific Model Development*, 9, 3461–3482. <https://doi.org/10.5194/gmd-9-3461-2016>
- Pai, D., Sridhar, L., Rajeevan, M., Sreejith, O., Satbha, N., Satbhai, N., & Mukhopadhyay, B. (2014). Development of a new high spatial resolution (0.25° 0.25°) long period (1901–2010) daily gridded rainfall data set over India and its comparison with existing data sets over the region. *Mausam*, 65, 1–18. <https://doi.org/10.54302/mausam.v65i1.851>
- Philip, S., Sparrow, S., Kew, S. F., van der Wiel, K., Wanders, N., Singh, R., et al. (2019). Attributing the 2017 Bangladesh floods from meteorological and hydrological perspectives. *Hydrology and Earth System Sciences*, 23(3), 1409–1429. <https://doi.org/10.5194/hess-23-1409-2019>
- Qu, X., & Huang, G. (2011). Impacts of tropical Indian Ocean SST on the meridional displacement of East Asian jet in boreal summer. *International Journal of Climatology*, 32(13), 2073–2080. <https://doi.org/10.1002/joc.2378>
- Rajeevan, M., Bhat, J., & Jaswal, A. (2008). Analysis of variability and trends of extreme rainfall events over India using 104 years of gridded daily rainfall data. *Geophysical Research Letters*, 35(18), L18707. <https://doi.org/10.1029/2008gl035143>
- Ramanathan, V., Chung, C., Kim, D., Bettge, T., Buja, L., Kiehl, J. T., et al. (2005). Atmospheric Brown clouds: Impacts on South Asian climate and hydrological cycle. *Proceedings of the National Academy of Sciences*, 102(15), 5326–5333. <https://doi.org/10.1073/pnas.0500656102>
- Rasmusson, E. M., & Carpenter, T. H. (1983). The relationship between eastern equatorial Pacific sea surface temperatures and rainfall over India and Sri Lanka. *Monthly Weather Review*, 111(3), 517–528. [https://doi.org/10.1175/1520-0493\(1983\)111<0517:trbeep>2.0.co;2](https://doi.org/10.1175/1520-0493(1983)111<0517:trbeep>2.0.co;2)
- Rayner, N. A., Parker, D. E., Horton, E. B., Folland, C. K., Alexander, L. V., Rowell, D. P., et al. (2003). Global analyses of sea surface temperature, sea ice, and night marine air temperature since the late nineteenth century. *Journal of Geophysical Research*, 108(D14), 4407. <https://doi.org/10.1029/2002jd002670>
- Rimi, R. H., Hausteine, K., Barbour, E. J., & Allen, M. R. (2019). Risks of pre-monsoon extreme rainfall events of Bangladesh: Is anthropogenic climate change playing a role? *Bulletin America Meteorology Social*, 100(1), S61–S65. <https://doi.org/10.1175/bams-d-18-0152.1>
- Singh, D., Ghosh, S., Roxy, M. K., & McDermid, S. (2019). Indian summer monsoon: Extreme events, historical changes, and role of anthropogenic forcings. *Wiley Interdisciplinary Reviews: Climate Change*, 10(2), e571. <https://doi.org/10.1002/wcc.571>
- Singh, D., Horton, D. E., Tsiang, M., Haugen, M., Ashfaq, M., Mei, R., et al. (2014). Severe precipitation in northern India in June 2013: Causes, historical context, and changes in probability. *Bulletin America Meteorology Social*, 95(9), S58–S61.
- Takaya, Y., Ishikawa, I., Kobayashi, C., Endo, H., & Ose, T. (2020). Enhanced Meiyu-Baiu rainfall in early summer 2020: Aftermath of the 2019 super IOD event. *Geophysical Research Letters*, 47(22), e2020GL090671. <https://doi.org/10.1029/2020gl090671>
- Tang, H., Wang, Z., Tang, B., Ma, Y., Pei, L., Tian, F., et al. (2022). Reduced probability of 2020 June–July persistent heavy Meiyu rainfall event in the mid-lower reaches of the Yangtze River basin under anthropogenic forcing. *Bulletin America Meteorology Social*, 103(3), S83–S89. <https://doi.org/10.1175/BAMS-D-21-0167.1>
- van Oldenborgh, G. J., Otto, F. E. L., Hausteine, K., & Achuta Rao, K. (2016). The heavy precipitation event of December 2015 in Chennai, India. *Bulletin America Meteorology Social*, 97(12), S87–S91. <https://doi.org/10.1175/bams-d-16-0129.1>
- Walker, G. (1924). Correlation in seasonal variations of weather. IV: A further study of world weather. *Mem Indian Meteorological Department*, 24(211), 275–332. <https://doi.org/10.1002/qj.49705021136>
- Wilks, D. (2006). Statistical Methods in the atmospheric Sciences, *International Geophysics Series*, (2nd ed., Vol. 91, p. 627). Elsevier.
- WMO News. (2020). *Heavy rains and flooding hit large parts of Asia*. Retrieved from <https://public.wmo.int/en/media/news/heavy-rains-and-flooding-hit-large-parts-of-asia>. Accessed 27 September 2021.
- Xie, P., Chen, M., Yang, S., Yatagai, A., Hayasaka, T., Fukushima, Y., & Liu, C. (2007). A gauge-based analysis of daily precipitation over East Asia. *Journal of Hydrometeorology*, 8(3), 607–626. <https://doi.org/10.1175/jhm583.1>
- Xie, S.-P., Kosaka, Y., Du, Y., Hu, K., Chowdary, J. S., & Huang, G. (2016). Indo-Western Pacific Ocean capacitor and coherent climate anomalies in post-ENSO summer: A review. *Advances in Atmospheric Sciences*, 33(4), 411–432. <https://doi.org/10.1007/s00376-015-5192-6>
- Yang, X., & Huang, P. (2021). Restored relationship between ENSO and Indian summer monsoon rainfall around 1999/2000. *The Innovation*, 2, 100102. <https://doi.org/10.1016/j.xinn.2021.100102>
- Zhang, L., Zhao, D., Zhou, T., Peng, D., & Xiao, C. (2021). Moisture origins and transport processes for the 2020 Yangtze River Valley record-breaking Mei-yu rainfall. *Advances in Atmospheric Sciences*, 38(12), 2125–2136. <https://doi.org/10.1007/s00376-021-1097-8>
- Zhang, W., Huang, Z., Jiang, F., Stuecker, M. F., Chen, G., & Jin, F. (2021). Exceptionally persistent Madden-Julian oscillation activity contributes to the extreme 2020 east Asian summer monsoon rainfall. *Geophysical Research Letters*, 48(5), e2020GL091588. <https://doi.org/10.1029/2020gl091588>

- Zhou, Z.-Q., Xie, S.-P., & Zhang, R. (2019). Variability and predictability of Indian rainfall during the monsoon onset month of June. *Geophysical Research Letters*, 46(24), 14782–14788. <https://doi.org/10.1029/2019gl085495>
- Zhou, Z.-Q., Xie, S.-P., & Zhang, R. (2021). Historic Yangtze flooding of 2020 tied to extreme Indian Ocean conditions. *Proceedings of the National Academy of Sciences*, 118(12), e2022255118. <https://doi.org/10.1073/pnas.2022255118>
- Zhou, Z.-Q., Zhang, R., & Xie, S.-P. (2019). Interannual variability of summer surface air temperature over central India: Implications for monsoon onset. *Journal of Climate*, 32(6), 1693–1706. <https://doi.org/10.1175/jcli-d-18-0675.1>